International Journal of Electrical, Electronic and Communication Sciences
ISSN: 2517-9438
Vol:13, No:4, 2019

Effect of Leaks in Solid Oxide Electrolysis Cells Tested for Durability under Co-Electrolysis Conditions

Megha Rao, Søren H. Jensen, Xiufu Sun, Anke Hagen, Mogens B. Mogensen

Abstract**—**Solid oxide electrolysis cells have an immense potential in converting CO_2 and H_2O into syngas during co-electrolysis operation. The produced syngas can be further converted into hydrocarbons. This kind of technology is called power-to-gas or power-to-liquid. To produce hydrocarbons via this route, durability of the cells is still a challenge, which needs to be further investigated in order to improve the cells. In this work, various nickel-yttria stabilized zirconia (Ni-YSZ) fuel electrode supported or YSZ electrolyte supported cells, cerium gadolinium oxide (CGO) barrier layer, and an oxygen electrode are investigated for durability under co-electrolysis conditions in both galvanostatic and potentiostatic conditions. While changing the gas on the oxygen electrode, keeping the fuel electrode gas composition constant, a change in the gas concentration arc was observed by impedance spectroscopy. Measurements of open circuit potential revealed the presence of leaks in the setup. It is speculated that the change in concentration impedance may be related to the leaks. Furthermore, the cells were also tested under pressurized conditions to find an inter-play between the leak rate and the pressure. A mathematical modeling together with electrochemical and microscopy analysis is presented.

Keywords**—**Co-electrolysis, solid oxide electrolysis cells, leaks, durability, gas concentration

I. Introduction

THE goal of reducing CO_2 emissions by 2050 in order to reduce its impact on global warming has paved way for renewable technologies to replace fossil fuels [1]. The most prominent renewable energy sources are reported to be wind and solar. However, given their intermittent nature energy storage is essential. Batteries are one of the leading storage devices in use nowadays, along with compressed-air and pumped hydro storage. Nevertheless, the excess energy produced from renewable sources can be stored in the form of hydrocarbons such as methane, methanol etc. This technology, known as Power-to-Gas (PtG) or Power-to-Liquid (PtL), has immense potential namely to produce hydrocarbons avoiding the fossil fuel route [2]. One of the storage technologies in this context is high temperature electrolysis using Solid Oxide Electrolysis Cells (SOECs) which has an advantage of converting CO_2 and H_2O into syngas through a process known as co-electrolysis, which can be further rendered into desired hydrocarbons downstream [3]. Another interesting aspect of using SOECs as reported is the formation of methane during co-electrolysis under pressurized conditions [4]. However, commercialization of SOECs is accompanied by the challenge of realizing a shelf life of 5-10 years. The cells tested for over 1000 hours have been analyzed for degradation as reported in literature. For the fuel electrode supported cells, most of the degradation studies have attributed the degradation of the fuel electrode via poisoning of Ni, impurities in the gas stream, loss in Ni percolation and migration of Ni particles thereby reducing the network of Ni for conduction of electrons [3], [5]-[8]. In addition, delamination of oxygen electrode has also been addressed in literature [3], [9], [10].

While testing the cells for durability, galvanostatic, i.e. constant current, mode of operation is preferred due to the ease of data analysis. However, this leads to an increase in electrode overpotential leading to faster degradation depending on the operating conditions. Potentiostatic, i.e. constant voltage mode is more reliable since the cells operate at constant voltage for instance, thermoneutral voltage which is useful from system point of view, and thereby protects the cells by keeping the overpotential on the cells constant [11].

It is of utmost importance to account for the magnitude of leaks while testing of the cells to have an accurate data analysis to understand the degradation mechanisms. In this work, cells are analyzed under high steam content (80-90% steam) and co-electrolysis conditions wherein a change in gas conversion arc was prominent. The cells were analyzed for diffusion and crossover. The results are presented at ambient pressure and compared with a test a under pressurized conditions. Furthermore, SEM analysis was carried out to investigate the leaks.

II. Experimetal

In this study, different types of fuel electrode supported cells were analyzed as listed below:

Cell A: Consisting of Ni-YSZ fuel electrode, YSZ electrolyte, lanthanum strontium manganite (LSM)-YSZ oxygen electrode, LSM contact layer.

Cell B: Consisting of Ni-YSZ fuel electrode, YSZ electrolyte, LSC:CGO oxygen electrode, LSM contact layer.

Cell C: Consisting of Ni-YSZ fuel electrode, YSZ electrolyte, CGO barrier layer, LSCF:CGO oxygen electrode.

Cell D: Consisting of Ni-YSZ fuel electrode, YSZ electrolyte, CGO barrier layer, LSC:CGO oxygen electrode.

Megha Rao is with the Technical University of Denmark, Risø, Roskilde, 4000 Denmark (phone: +4593511857; e-mail: mrao@dtu.dk).

Søren H. Jensen is with Hybrid Greentech ApS, Risø, 4000, Denmark (e-mail: shjj@dtu.dk).

Xiufu Sun, Anke Hagen, and Mogens B. Mogensen are with the Technical University of Denmark, Risø, Roskilde, 4000 Denmark (e-mail: xisu@dtu.dk, anke@dtu.dk, momo@dtu.dk).

Cell E: Consisting of Ni-YSZ fuel electrode (optimized particle size distribution as compared to Cell-D), YSZ electrolyte, CGO barrier layer, LSC:CGO oxygen electrode.

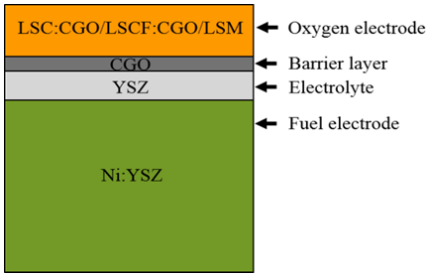

Fig. 1 Depiction of cells used for testing and analysis

The cells were 4* 4 cm^2 area. The cross-section is illustrated in Fig. 1. Tests were carried out in a setup as reported in literature [8], [12]. The cells were mounted in an alumina cell test house. Gold and nickel were used as current collector contact on the oxygen and fuel side, respectively. A gold sealing was used on the fuel side. 4 kilograms of weight was applied on top of the cell house during start up to ensure that the sealants were gas tight and to ensure good electrical contact between the cell and the contact components. The cells were reduced according to the procedure reported in literature [5]. Electrochemical characterization (fingerprint) of the cell was performed afterwards.

The fingerprint is a standardized electrochemical characterization of the cells ranging from 850 ^oC down to 650 ^oC, depending on the test. At selected temperatures, i-V characterization and EIS measurements were performed with air or O_2 supplied to the oxygen electrode, and with 4%, 20%, 50%, 80%, or 90% steam in H_2 to the fuel electrode. Additionally, characterization in co-electrolysis gas mixture was carried out for some of the cells with 45% H_2O + 45% CO_2 + 10% H_2 and 65% H_2O + 25% CO_2 + 10% H_2 supplied to the fuel electrode.

EIS measurements were carried out under open circuit voltage (OCV) condition, using a Solartron frequency analyzer and an external shunt resistor in series with the cell. The spectra were recorded from 96,850 to 0.08 Hz, with 12 points per decade. Thereafter, the spectra were compensated using the short circuit impedance response of the test setup. A short-circuit impedance response for compensation of EIS was measured without the cell test house. From the impedance spectra, the ohmic resistance of the cell (serial resistance, Rs) was taken as the value of the real part of the impedance at 96,850 Hz. The polarization resistance (Rp) was then calculated as the difference of the real part of the impedance at 96,850 Hz and 0.08 Hz. i-V curves were recorded both in fuel cell (FC) and electrolysis (EC) mode with the above-mentioned gas compositions. For FC mode, the minimum voltage limit was set to 650 mV, while for EC mode the curve maximum voltage was set to 1,300 mV. Analysis of the impedance data was performed using the software Ravdav [13].

Post-test analysis of the cells was performed using scanning electron microscopy (SEM). Polished cross-sections along the hydrogen/steam flow path from inlet to outlet were prepared for all cells. The cell microstructure was examined using a Supra-35 scanning electron microscope (SEM) equipped with a field emission gun (FE-SEM, Carl Zeiss) and an energy-dispersive X-ray spectrometer (EDS, Thermo Electron Corporation). The samples were embedded in epoxy and carbon coated to avoid charging of the sample surface and to ensure a grounded connection. Backscatter and Secondary electron (SE-2) detector are used for imaging.

III. Results and Discussion

The fingerprints of the cells were analyzed to the effect of gas conversion and to identify the response of fuel and oxygen electrodes. For this purpose, impedance curves were plotted. During the testing of cells, prominent leaks were observed under high steam conditions and co-electrolysis conditions. Two such cases are displayed in Fig 2. In Fig. 2 (a), Cell type-E is tested under co-electrolysis conditions with 65% H_2O + 25% CO_2 + 10% H_2 on the fuel electrode, while on the oxygen electrode a shift from oxygen to air is performed. It is evident that the impedance is higher when the cell is tested with oxygen. In Fig. 2 (b), Cell type-B is tested under co-electrolysis conditions with 65% H_2O + 25% CO_2 + 10% H_2 on the fuel electrode, while on the oxygen electrode a gas shift from oxygen to air is performed. Similar to Fig. 2 (a), the impedance is higher in oxygen. The resistance should be lower or almost similar in oxygen to that in air, since the fuel electrode composition remains the same.

To identify the frequency of the process occurring with change in oxygen electrode gas shift, distribution of relaxation times (DRT) analysis is performed [14]. The DRT analysis performed for the Nyquist plots is shown in Fig. 3.

During change of gas from oxygen to air, keeping the fuel flow constant, a change in impedance spectra was observed at low frequency which is clearly seen in the DRT plot at a frequency of approximately 1 Hz, assigned to the gas concentration resistance as previously reported in literature [15]. However, the gas concentration resistance was higher in oxygen than in air, which seems counter intuitive. The result indicates leaks leading to change in the gas composition to a greater extent with pure oxygen as compared to air. To further explain this, if oxygen is leaking such to the fuel side through a pinhole for instance, it can react with H_2 to form H_2O, thereby changing the ratio of H_2 present which is clearly represented by the gas concentration arc. Moreover, due to the calculation of Nernst potential, a change in gas conversion is more susceptible and visible at high steam content [16].

Following this, a comprehensive analysis on the origin and extent of leaks was performed. To begin with, the case of gas diffusion is analyzed, wherein the leaks only through the pinholes are considered, which in turn indicates diffusion of O_2 from the oxygen to fuel electrode and diffusion of H_2 from fuel to oxygen electrode such that the ratio of steam to H_2 is modified in the fuel electrode. It is assumed that the leak is due to only diffusion, either of O_2 or of H_2 gas or both simultaneously. An illustration of leak by diffusion through a

pinhole is displayed in Fig. 4.

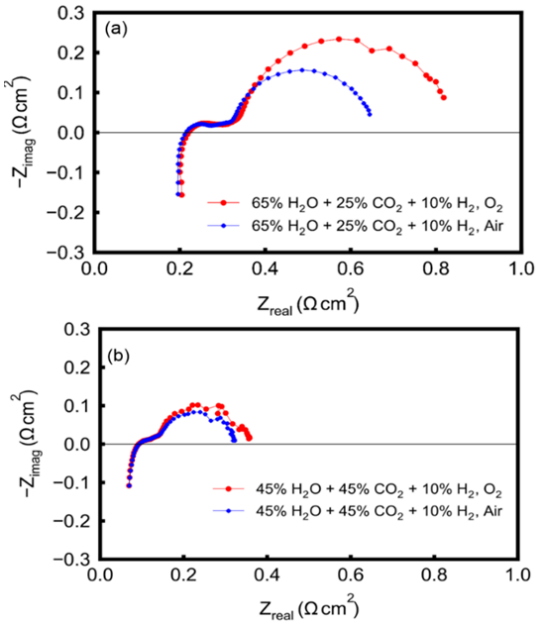

Fig. 2 Gas shift analysis on oxygen electrode under co-electrolysis conditions (a) Cell type-E with 65% H_2O + 25% CO_2 + 10% H_2 on the fuel electrode, (b) Cell type-B with 45% H_2O + 45% CO_2 + 10% H_2 on the fuel electrode

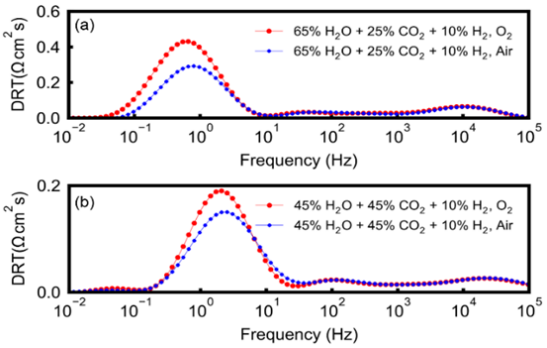

Fig. 3 DRT analysis with a shift from oxygen to air on the oxygen electrode under co-electrolysis conditions (a) Cell type-E with 65% H_2O + 25% CO_2 + 10% H_2 on the fuel electrode, (b) Cell type-B with 45% H_2O + 45% CO_2 + 10% H_2 on the fuel electrode

Firstly, the change in OCV was calculated such that:

$$\Delta OCV = OCV_{Nernst} - OCV_{measured} \quad (1)$$

This is calculated for both oxygen and air cases, keeping the fuel composition constant. Moreover,

$$\Delta OCV_{sub} = \Delta OCV_{O2} - \Delta OCV_{Air} \quad (2)$$

ΔOCV_{sub} is a measure of difference in the air and oxygen OCVs which will be utilized to calculate the leak.

Table I summarizes the findings for all the cells described in Experimental section with the OCV differences. Here, cell type represents the type of cell defined in the experimental section along with a number to identify the cell for future reference. For the case of Cell-A, A1, A2 and A3 were tested under different conditions as displayed in Table I.

Considering, two extreme cases of only hydrogen and only oxygen diffusion as shown in Fig. 5 is obtained. For the case of pure hydrogen leak, where only H_2 is diffusing through the pinhole, there would be equal leaks in both air and oxygen. For the case of pure oxygen leak, implying only O_2 diffusing through the pinhole, the diffusion would depend on the partial pressure of oxygen and for the case of air, the amount of oxygen diffused would be 0.21 times that of pure oxygen. The change in OCV differences thus obtained according to the equation below.

$$\Delta OCV_{diff} = (\Delta OCV_{O2} - \Delta OCV_{Air}) - (\Delta OCV_{O2,new} - \Delta OCV_{Air}) \quad (3)$$

where, $OCV_{O2,new}$ is the calculated OCV in O_2 assuming pure O_2 leak, based on the $OCV_{Air,measured}$

ΔOCV_{diff} is the deviation from the change in the theoretical value when assuming pure oxygen leak based on the fact that the OCV measured in air is only due to the oxygen leak. The calculations performed in (2) and (3) help in better understanding of the deviation of leaks when only diffusion of one gas is considered:

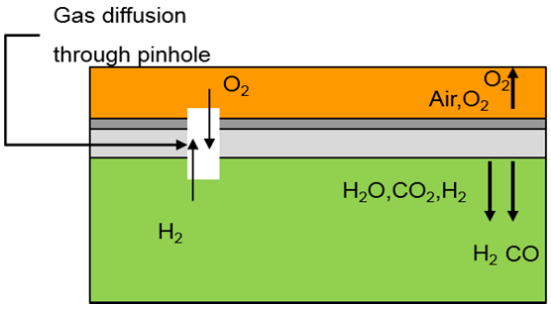

Fig. 4 Illustration of diffusion of gas through pinhole through the electrodes and electrolyte for diffusion

Considering (2) and (3) to calculate the deviation for pure hydrogen and pure oxygen leak in Table I, it was found out that the data was scattered and did not agree either with pure H_2 or pure O_2 leak, which led to the possibility of both gases diffusing simultaneously through the pinhole. The values which are empty in the table represent that the case of pure oxygen diffusion will not be valid here since the leak would be excessive.

Furthermore, the values for leak currents under both conditions, is presented in Table II. The values which are empty are due to the incomplete data availability or inaccuracy of the testing conditions, so they are disregarded. These values are taken as 0 in Fig. 6.

TABLE I
CHANGE IN OCV FOR DIFFERENT CELL TYPES

Cell type	Fuel electrode composition	ΔOCV_{O2} (mV)	ΔOCVair (mV)	ΔOCVsub (mV)	ΔOCVdiff (mV)
A1	45%CO_2+45%H_2O+10%H_2	12.5	9.4	3.1	
A2	45%CO_2+45%H_2O+10%H_2	14.7	10.9	3.8	85.4
A3	45%CO_2+45%H_2O+10%H_2	106.7	119.4	-12.7	83.4
B1	45%CO_2+45%H_2O+10%H_2	29.5	20.5	8.9	
B2	80%H_2O+20%H_2	10.3	9.1	1.2	
B3	80%H_2O+20%H_2	16.4	11.1	5.3	19.9
B4	80%H_2O+20%H_2	28.6	19.1	9.5	17.9
C1	45%CO_2+45%H_2O+10%H_2	9.9	8.1	1.8	106.6
C2	45%CO_2+45%H_2O+10%H_2	23.6	14.6	9	
C3	45%CO_2+45%H_2O+10%H_2	9.6	6.7	2.9	55.2
C4	45%CO_2+45%H_2O+10%H_2	11	7.6	3.4	84.3
C5	45%CO_2+45%H_2O+10%H_2	19.8	13.4	6.3	107.1
D1	90%H_2O+10%H_2	12.9	4.5	8.4	
E1	25%CO_2+65%H_2O+10%H_2	29.1	7.7	21.4	

Following this, diffusion is further investigated. Diffusion coefficients are calculated for binary and multicomponent mixtures. Knudsen, Binary and Stefan-Maxwell diffusion models are considered in this work. Using Kinetic Theory of Gases, Knudsen diffusion coefficient is calculated as:

$$D_{i,K}^{eff} = \frac{\epsilon}{\tau}\frac{d_p}{3}\sqrt{\frac{8RT}{\pi M_i}} \quad (4)$$

where, M_i is the molecular weight of component i, d_p is the pore diameter, ε is the electrode porosity and τ is the electrode tortuosity.

For the calculation of Binary diffusion coefficient, Chapman-Enskog correlation is used as follows:

$$D_{i,j}^{eff} = \frac{\epsilon}{\tau}D_{i,j} = \frac{\epsilon}{\tau}0.001858\,T^{1.5}\frac{\left(\frac{1}{M_i}+\frac{1}{M_j}\right)^{0.5}}{p\sigma_{i,j}^2\Omega_D} \quad (5)$$

where, T is the temperature, M_i and Mj are molecular weights of species i and j, p is the pressure, $\sigma_{i,j}$ is the average collision diameter between the species i and j and Ω_D us the dimensionless collision integral calculated using Lennard-Jones model. σ and Ω values are taken from literature [17], [18]. The values of ε and τ are taken from reported values in literature [19].

For the calculation of diffusion in multicomponent mixtures, Stefan Maxwell diffusion coefficient is calculated as follows:

$$D_{SM} = \sum\frac{1-y_i}{\frac{y_j}{D_{ij}}+\frac{y_k}{D_{ik}}} \quad (6)$$

where y represents the mole fraction of species and D is the binary diffusion coefficient calculated in (5).

Moreover, to analyze the nature of leaks, equivalent leak currents are calculated as follows:

$$Number\ of\ moles = \frac{Excess\ O2\ (L/h)}{22.4\ L/mol} \quad (8)$$

$$Leak\ current = \frac{Number\ of\ moles\ (mol/h) * F\ (A\,s/mol) * 4}{3600 * 16\ cm^2} \quad (9)$$

where, F is the Faraday constant, and 4 refers to the number of electrons per mole of excess O_2 gas.

Consequently, leak currents are calculated under these cases and leak current in air is plotted vs oxygen to understand the trend in oxygen and hydrogen leaks. In all the figures, similar cell types are represented together, i.e. all cells for cell type A have the same marker in plots.

In Fig. 5, all cell types are plotted to understand the relation between leaks in air and oxygen. Two trends line are shown: Trend 1 depicts pure hydrogen leak and Trend 2 depicts pure oxygen leak. The cells do not have pure hydrogen or pure oxygen leaks, which indicates the combination of both hydrogen and oxygen leak.

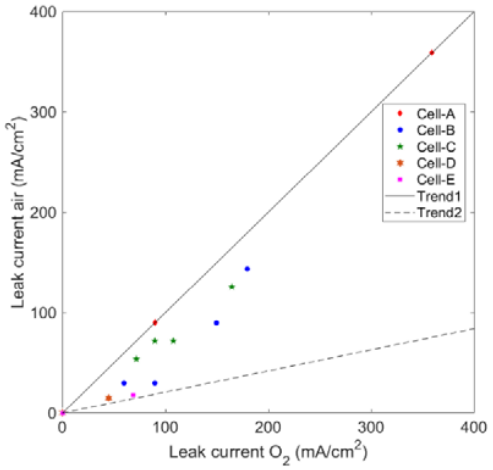

Fig. 5 Leak current in air vs leak current in oxygen for all the cells analyzed under co-electrolysis and steam electrolysis conditions

To further analyze the dependency of leaks, leaks are calculated according to (8) and (9) at 50% H_2O + 50% H_2 conditions on the fuel electrode while changing the gas from oxygen to air on the oxygen electrode.

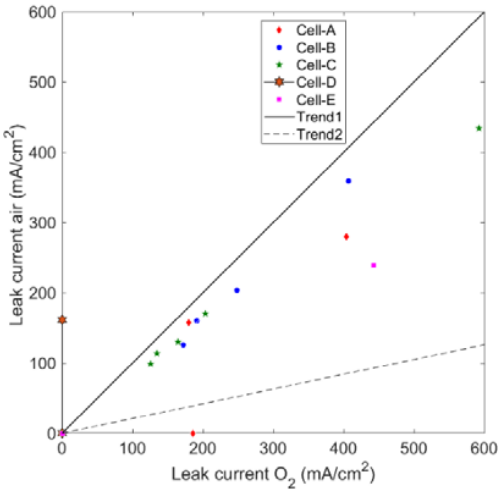

Fig. 6 Leak current in air vs leak current in oxygen for all the cells analyzed with 50%H_2O+50%H_2 on the fuel electrode

For the case of pure H_2 leak, the leak currents should be equal which is seen for Cell-A in Fig. 5. However, in Fig. 6 this theory is not consistent. Furthermore, for the case of pure O_2 leak, the ratio between leak currents should be related to the partial pressure of the O_2 present. The leak is significantly lower and there is no clear correlation. As a result, the leaks are due to both H_2 and O_2 diffusion.

Hence, the leaks are dependent on diffusion and flow. Revisiting Fig. 4, it can now be seen that the gases diffuse through pinholes. Furthermore, higher the flow, higher is the leak, which might be due to convection, with increase in gas crossover at higher flow rates.

Once the diffusion coefficients are calculated, to address the leaks, it is assumed that the ratio of hydrogen is changed (hydrogen and oxygen combust to form steam), considering the diffusion coefficients and molar fractions. This is done according to the following equation:

$$H_{2_{flow,measured}} = H_{2_{flow,theoretical}} - aD_{H_2}\chi_{H_2} - 2aD_{O_2}\chi_{O_2} \quad (7)$$

where, a is the variable which will be calculated for each test which is analyzed to find a correlation between leaks and diffusion. The a values are measured for both oxygen and air cases, wherein χ_{O2} is 1 for oxygen and 0.21 for air and χ_{H2} is 0.1 or 0.2 depending on the test. This is displayed in Fig. 7.

The line with slope = 1 indicates the case of pure diffusion shown by Trend. Moreover, the values of a for Cell-A type lie on the pure diffusion line and hence are not visible on the plot. There is a good scatter in the data acquired which leads to the understanding that both hydrogen and oxygen diffusion are occurring, but there are other factors to be considered regarding the leaks. Additionally, an offset is seen which can not be accounted for through diffusion.

Additionally, leaks under steam electrolysis are further addressed regarding the pressurized test. For the pressurized test, analysis is carried out based on the data collected in literature under 50% H_2O + 50% H_2 on the fuel electrode and air on the oxygen electrode [20]. The pressure dependency of leak current is displayed in Fig. 8.

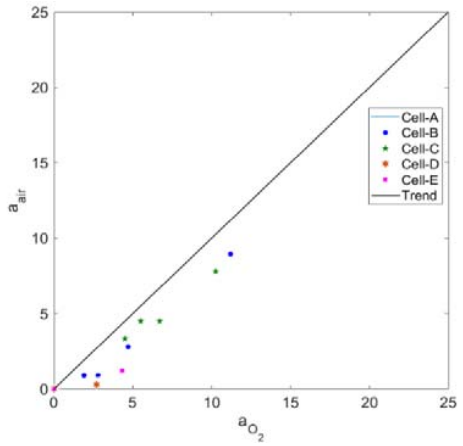

Fig. 7 Values of a in air are plotted vs a in oxygen for all the cells analyzed under steam and co-electrolysis conditions (Cell-A line overlaps with the trend completely)

TABLE II
LEAK CURRENTS FOR DIFFERENT CELL TYPES

Cell Type	Fuel electrode composition	Leak current in O_2 (mA/cm^2)	Leak current in air (mA/cm^2)
A1	45%CO_2+45%H_2O+10%H_2	89.7	89.7
	50%H_2O+50%H_2	179.5	157
A2	45%CO_2+45%H_2O+10%H_2	89.7	89.7
	50%H_2O+50%H_2	185.5	
A3	45%CO_2+45%H_2O+10%H_2	358.9	358.9
	50%H_2O+50%H_2	403.8	279.7
B1	45%CO_2+45%H_2O+10%H_2	179.5	143.6
	50%H_2O+50%H_2	406.8	358.9
B2	80%H_2O+20%H_2	59.8	29.9
	50%H_2O+50%H_2	172	125.6
B3	80%H_2O+20%H_2	89.7	29.9
	50%H_2O+50%H_2	191.4	160
B4	80%H_2O+20%H_2	149.6	89.7
	50%H_2O+50%H_2	248.3	203.4
C1	45%CO_2+45%H_2O+10%H_2	89.7	71.8
	50%H_2O+50%H_2	134.6	113.7
C2	45%CO_2+45%H_2O+10%H_2	164.5	175.6
	50%H_2O+50%H_2	592.3	433.7
C3	45%CO_2+45%H_2O+10%H_2	71.8	53.8
	50%H_2O+50%H_2	125.6	98.7
C4	45%CO_2+45%H_2O+10%H_2	89.7	71.8
	50%H_2O+50%H_2	164.5	130.1
C5	45%CO_2+45%H_2O+10%H_2	107.7	71.8
	50%H_2O+50%H_2	203.4	170.5
D1	90%H_2O+10%H_2	44.9	15
	50%H_2O+50%H_2		161.5
E1	25%CO_2+65%H_2O+10%H_2	68.8	17.9
	50%H_2O+50%H_2	442.7	239.3

This led to the investigation of pressure dependency of leaks. During pressure test, there different types of leaks may be encountered namely:

1. A pressure independent Stefan-Maxwell diffusion leak

2. A pressure dependent Knudsen leak

Considering diffusion case as done previously in this work, Maxwell diffusion and Knudsen diffusion are taking place simultaneously in the pressurized system, wherein the total diffusion constant is determined according to the following equation:

$$\frac{1}{D_{total}} = \frac{1}{D_{SM}} + \frac{1}{D_k} = \frac{P}{D_{SM}^0} + \frac{1}{D_k} \quad (10)$$

where, D_{SM} and D_k are calculated (4)-(6).

D_{SM} is dependent inversely on pressure and this is represented by pressured independent term D_{SM}^0, while D_k is independent of pressure. Furthermore, to calculate the rate of diffusion under pressure, the following equation is used:

$$J = D_{total}\nabla C = D_{total}\nabla C^0 P \quad (11)$$

where, ∇C is the concentration gradient which is pressure dependent, while ∇C^0 is the pressure independent concentration gradient.

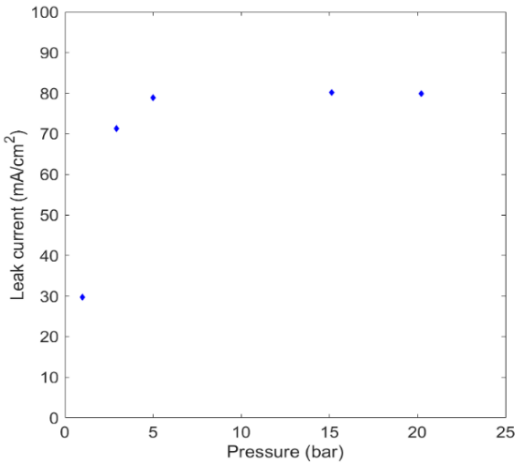

Fig. 8 Leak current vs pressure for a stack tested at 50% H_2O + 50% H_2 on fuel electrode and air on oxygen electrode

From (10) and (11), it is seen that to calculate the rate of diffusion, pressure terms cancel out for the case of Stefan-Maxwell diffusion making it pressure independent, while the Knudsen diffusion rate is proportional to the pressure. To fit the data in Fig. 9, an accurate contribution from Stefan-Maxwell and Knudsen diffusion needs to be found out using coefficients, which is not performed in this work.

Based on the electrochemical analysis on the data obtained from various tests, there is a significant leak present in all the cell tests analyzed in this work, which can be attributed to both diffusion and flow of gases crossing over. To substantiate the hypothesis, post-test SEM images of some of the tests are displayed in Fig. 9.

In Figs. 9 (a) and (b), backscatter images of cells with cracks in the electrolyte are presented. In Fig. 9 (a), the grain boundary crack is visible leading to the leaks in the cell. In Fig. 9 (b), a magnified image shows the pinholes present in the cell through which diffusion of hydrogen and oxygen are taking place. Fig. 9 (c) presents the extreme case of cracks formed in the cell during testing. The cracks go all the way through the electrolyte to the fuel electrode. This leads to an increase in leaks. To summarize, the leaks caused by the cracks could be due to pinhole diffusion as well as gas crossover due to pressure difference.

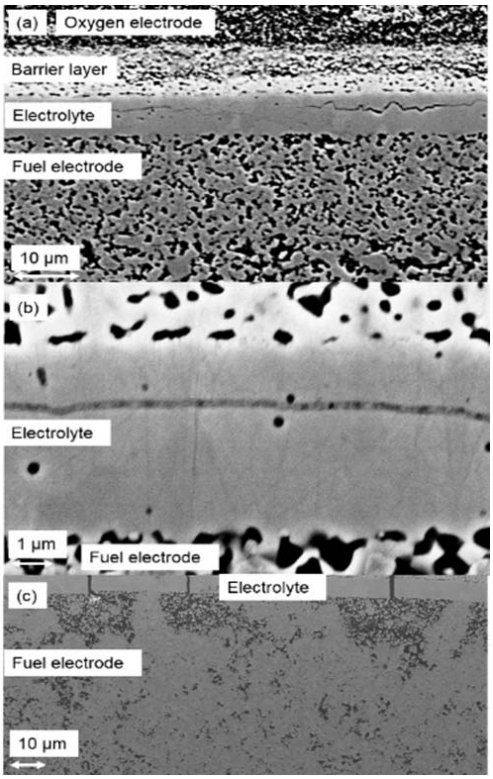

Fig. 9 SEM images displaying pinholes and cracks in the tested cells, (a)grain boundary crack in the electrolyte-backscatter detector, (b) pinholes in the electrolyte-backscatter detector, and (c)cracks in the fuel electrode through the electrolyte-SE-2 detector

IV. Conclusions

In this work, a leak analysis on cells tested for electrolysis and co-electrolysis was performed to understand the origin of leaks. The leaks were indicated to be a combination of both hydrogen and oxygen gas diffusion. Moreover, a flow dependency of the leaks was also indicated implying an increase in gas crossover at higher flow rates. Furthermore, for the case of pressurized system, the overall diffusion coefficient was also modeled for such a case. To substantiate the leaks, post-test SEM analysis revealed grain boundary cracks, cracks and pinholes in the tested cell.

Acknowledgment

The authors wish to thank Dr. Anne Hauch, Karen Brodersen, Søren Koch and Henrik Henriksen for technical help. The research leading to these results has received funding from the European Union's Horizon 2020 framework

program (H2020) for the Fuel Cells and Hydrogen Joint Technology Initiative under grant agreement no. 699892 ("Efficient Co-Electrolyser for Efficient Renewable Energy Storage-ECo").

REFERENCES

[1] European Commission, "Roadmap 2050," *Policy*, no. April, pp. 1–9, 2012.
[2] S. Mesfun, D. L. Sanchez, S. Leduc, E. Wetterlund, J. Lundgren, M. Biberacher, F. Kraxner, "Power-to-gas and power-to-liquid for managing renewable electricity intermittency in the Alpine Region," *Renew. Energy*, vol. 107, pp. 361–372, July 2017.
[3] X. Sun, M. Chen, Y.-L. Liu, P. Hjalmarsson, S.D. Ebbesen, S.H. Jensen, M. B. Mogensen, P. V. Hendriksen, "Durability of Solid Oxide Electrolysis Cells for Syngas Production," *J. Electrochem. Soc.*, vol. 160, no. 9, pp. F1074–F1080, July 2013.
[4] S. H. Jensen, H. Langnickel, N. Hintzen, M. Chen, X. Sun, A. Hauch, G. Butera, L. R. Clausen, "Pressurized reversible operation of a 30-cell solid oxide cell stack using carbonaceous gases,", *Proc. of EFC 2017*.
[5] A. Hauch, K. Brodersen, M. Chen, and M. B. Mogensen, "Ni/YSZ electrodes structures optimized for increased electrolysis performance and durability," *Solid State Ionics*, vol. 293, pp. 27–36, Oct. 2016.
[6] M. Chen, Y. L.Liu, J. J. Bentzen, W. Zhang, X.Sun, A. Hauch, Y. Tao, J. R. Bowen, P. V. Hendriksen, "Microstructural Degradation of Ni/YSZ Electrodes in Solid Oxide Electrolysis Cells under High Current," *J. Electrochem. Soc.*, vol. 160, no. 8, pp. F883–F891, May 2013.
[7] A. Hauch, S. D. Ebbesen, S. H. Jensen, and M. Mogensen, "Solid Oxide Electrolysis Cells : Microstructure and Degradation of the Ni / Yttria-Stabilized Zirconia Electrode," pp. 1184–1193, Sep 2008.
[8] S. D. Ebbesen, C. Graves, A. Hauch, S. H. Jensen, and M. Mogensen, "Poisoning of Solid Oxide Electrolysis Cells by Impurities," *J. Electrochem. Soc.*, vol. 157, no. 10, p. B1419, Aug 2010.
[9] P. Hjalmarsson, X. Sun, Y. L. Liu, and M. Chen, "Influence of the oxygen electrode and inter-diffusion barrier on the degradation of solid oxide electrolysis cells," *J. Power Sources*, vol. 223, pp. 349–357, Feb 2013.
[10] V. Gil, K. K. Hansen, "High Performance Infiltrated Backbones for Cathode-Supported SOFC's," *ECS* Tans., 2014.
[11] M. Rao, X. Sun, and A. Hagen, "A Comparative Study of Durability of Solid Oxide Electrolysis Cells Tested for Co-Electrolysis under Galvanostatic and Potentiostatic Conditions," *J. Electrochem. Soc.,* vol. 165, no. 10, pp. 748–755, June 2018.
[12] S. H. Jensen, A. Hauch, P. V. Hendriksen, and M. Mogensen, "Advanced Test Method of Solid Oxide Cells in a Plug-Flow Setup," *J. Electrochem. Soc.*, vol. 156, no. 6, p. B757, Apr. 2009.
[13] C. Graves, "Ravdav." Department of Energy Conversion and Storage, Technical University of Denmark, 2012.
[14] S. H. Jensen, J. Hjelm, A. Hagen, and M. Mogensen, "Electrochemical impedance spectroscopy as diagnostic tool," in Handb. Fuel Cells., vol. 6, John Wiley & Sons, 2009.
[15] S. H. Jensen, A. Hauch, P. V. Hendriksen, M. Mogensen, N. Bonanos, and T. Jacobsen, "A Method to Separate Process Contributions in Impedance Spectra by Variation of Test Conditions," *J. Electrochem. Soc.*, vol. 154, no. 12, p. B1325, Oct. 2007.
[16] S. Primdahl, M. Mogensen, "Gas Conversion Impedance: A Test Geometry Effect in Characterization of Solid Oxide Fuel Cell Anodes," vol. 145, no. 7, pp. 2431–2438, Mar. 1998.
[17] M. García-Camprubí, N. Fueyo, V. Novaresio, P. Asinari, and S. Izquierdo, "An open-source library for the numerical modeling of mass-transfer in solid oxide fuel cells," *Comput. Phys. Commun.*, vol. 183, no. 1, pp. 125–146, Aug, 2011.
[18] E. Hernández-Pacheco, D. Singh, P. N. Hutton, N. Patel, and M. D. Mann, "A macro-level model for determining the performance characteristics of solid oxide fuel cells," *J. Power Sources*, vol. 138, no. 1–2, pp. 174–186, Aug. 2004.
[19] J. Dragsbæk Duhn, A. Degn Jensen, S. Wedel, and C. Wix, "Modeling of Gas Diffusion in Ni/YSZ Electrodes in CO2 and Co-electrolysis," *Fuel Cells*, vol. 17, no. 4, pp. 442–456, July 2017.
[20] S. H. Jensen, X. Sun, S. D. Ebbesen, and M. Chen, "Pressurized Operation of a Planar Solid Oxide Cell Stack," *Fuel Cells*, vol. 16, no. 2, pp. 205–218, Feb. 2016.